Solid State Ionics 207 (2012) 1–13

Contents lists available at SciVerse ScienceDirect

Solid State Ionics

journal homepage: www.elsevier.com/locate/ssi

Review

Ionic diffusion as a matter of lattice-strain for electroceramic thin films

Jennifer L.M. Rupp *

National Institute of Materials Science (NIMS), Research Center for Materials Nanoarchitectonics (MANA), 1-1 Namiki, Tsukuba, Ibaraki 305-0044, Japan

ARTICLE INFO

Article history:
Received 15 February 2011
Received in revised form 12 September 2011
Accepted 15 September 2011
Available online 10 December 2011

Keywords:
Strain
Ionic conductivity
Metal oxide
Ceria
Zirconia
CGO
Thin film
MEMS

ABSTRACT

Ionic conducting metal oxide thin films for Si-wafer based electroceramic devices are of high relevance to allow for new applications, quicker response times, and higher efficiencies. Metal oxide thin films are deposited via various processes on substrates. Depending on the synthesis method their microstructures differ on an atomistic length scale in their anionic and cationic lattice displacement fields and packing densities. Local changes in ionic bond strength can affect the oxygen migration barriers and ionic diffusion is no longer to be assumed as equal to zero-strained bulk material. This article proposes *lattice strain* measurements to characterize the defect states of metal oxide thin films that depend on their processing history and to correlate this measure for atomistic disorder. It is suggested to discuss differences in ionic conductivity observed relative to lattice strain and atomistic disorder in addition to other microstructure characteristics such as the grain size. The interplay of grain size, degree of crystallinity, phase changes and ionic conductivity are discussed with respect to lattice-strain for state-of-the-art ionic conducting thin films, i.e. ceria or zirconia solid solutions. Previous findings on the fields of compressive or tensile strain in epitaxial heterolayers or free-standing membrane films are discussed and compared with processing-dependent lattice strain of fully crystalline ceramic thin films of more than 200 nm in thickness. Finally, guidelines for processing of highly strained films with high ionic conduction are given for functional oxide thin films in Si-based electroceramic devices.

Contents

1. Introduction

Electrical conducting and dielectric metal oxide thin films are required for Si-wafer based electroceramic devices such as gas sensors [1–3], micro-solid oxide fuel cell membranes [4–10] or oxygen pumps [11]. These devices typically consist of electroceramic thin films integrated on a Si- or glass-ceramic-based wafer substrate in the form of a supported or free-standing membrane structure to allow for high sensing or power performance. The major challenge in this Si-based electroceramic device fabrication is the combination of choosing adequate thin film deposition techniques for the functional layers, and compatible processes for the overall device microstructuring [12]. Typically, the thin films are deposited and post-annealed between room temperature and 800 °C to avoid severe damage of the Si-wafer substrate [13]. Whereas for ferroelectric and magnetic thin films many examples of the correlation between the strain state, their properties and the low temperature processing are documented [14–20], first

* Current address: Massachusetts Institute of Technology (MIT), Department of Materials Science and Engineering and Department of Nuclear Science and Engineering, office NW13-221, 77 Massachusetts Ave, Cambridge, MA 02139, USA. Tel.: +81 298604896; fax: +81 298604706.
E-mail address: RUPP.Jennifer@nims.go.jp.

0167-2738/$ – see front matter © 2011 Elsevier B.V. All rights reserved.
doi:10.1016/j.ssi.2011.09.009

knowledge on the interplay of strain and ionic conduction for electroceramic thin films is just published [21–23]. Classic ionic conducting electroceramic thin films are yttria-stabilized zirconia and gadolinia-doped ceria in air. Their respective conductivity in air results from oxygen ions migrating via oxygen vacancies in the crystal lattice [24–26]. Recently, Kushima and Yildiz pointed out that the ionic diffusion migration barrier of yttria-stabilized zirconia can alter upon tensile lattice strain through density functional theory and nudged elastic band computation [21]. On an atomistic view *lattice strain* can affect the local change in space along the ionic migration path and the interatomic bond strength between the migrating oxygen and the nearest neighbor cation [21]. It is important to note that strain can possibly weaken or strengthen the interatomic bond strengths in a crystal lattice of: i. cation–cation, ii. cation–oxygen vacancy, or, iii. oxygen vacancy–oxygen vacancy [21–23]. Strong changes in the anionic and cationic lattice positions through elastic stretching may even lead to local bond breaks or relaxations, oxygen trapping and reordering processes such as a new phase formation or changes in non-stoichiometry. Lubomirsky and co-workers reported that the strain states affect the presence of oxygen vacancies and chemical bond strength through changes in the elastic "Young's" modulus of free-standing undoped and doped ceria thin film membranes [27–33]. Neutron diffraction experiments and reverse Monte Carlo modeling on undoped ceria by Hull et al. [34], and on yttria- and scandia-doped-zirconia by Norberg et al. [35] and Marrocchelli et al. [36] revealed that changes in ionic bond strength due to lattice strain affect oxygen vacancy pair coupling along <111> direction in these CaF_2 sintered ceramics. The consequences were a hampered ionic diffusion and reduction of the ionic conductivity. This was explicitly reported for a high non-stoichiometry in ceria, and for substitution of the solute scandia in the zirconia lattice by yttria of larger ionic radii size. In general, these very recent reports demonstrate that the oxygen migration barrier of classic ionic conducting electroceramics such as zirconia- or ceria-based materials can vary with respect to lattice strains.

A suitable working hypothesis for *electroceramic thin films* is that the choice in the processing route, e.g. temperature, oxygen partial pressure and chemistry conditions affects the local variations of ionic bond strengths in the crystal lattices giving rise to different levels of *lattice-strain*. Specifically, *lattice-strain* describes the long range isotropic displacement fields of the atoms in a material [37–39] and is also often referred to as "microstrain" in literature [40–42], Fig. 1a. In strained regions the cationic and/or the anionic lattice positions can be off-centered compared to a zero-strained bulk ceramic. These processing-related different levels of lattice strain in a thin film can impose: (i.) compressive, (ii.) tensile, or (iii.) mixed states with local compressive and tensile regions over the different unit cells of a polycrystalline ceramic thin film. Lattice strain in ionic conducting thin films can potentially alter the total ionic migration barrier i.e. through (i.) re-ordering of oxygen vacancies relative to cationic positions, or (ii.) formation of oxygen vacancy pairs along specific unit crystal directions. Also, interatomic bond braking upon high non-elastic strains has to be taken into account.

To *measure the lattice strain of an electroceramic thin film* the following techniques may be considered: state-of-the-art experimental

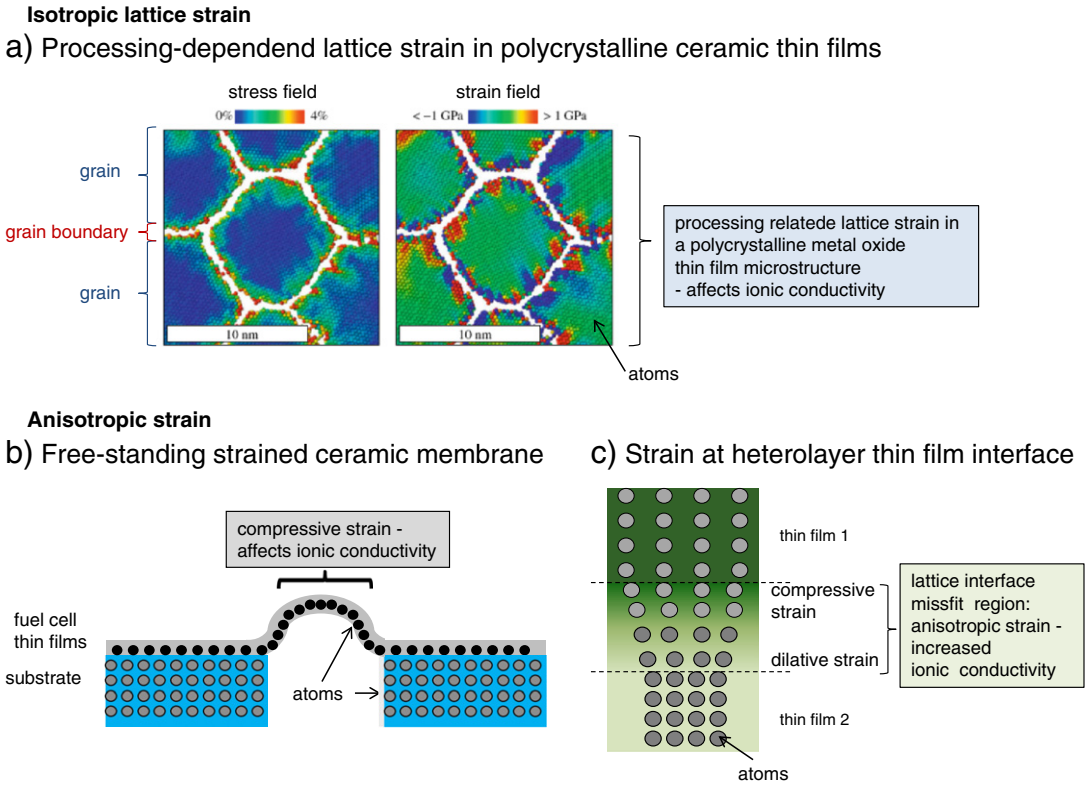

Fig. 1. Schematic view of anisotropic- and isotropic-strain fields for ionic conducting metal oxides. *Lattice strain* describes the isotropic long range atomic displacement fields and local variations in ionic bond strengths in metal oxide thin films relative to processing history [43], a. In contrast anisotropic-strain fields are clearly tensile or compressive, and therefore directed, b and c. The following examples are given for lattice strain: (a) Metal oxide films reveal different amounts of lattice strain dependent on the thin film processing and annealing conditions. The strain is distributed over the grain–grain boundary microstructure and represents a long range isotropic displacement field. We report in this article on literature examples where strain is increased for low temperature processed films, and ionic conductivity increases. Typical film thicknesses considered are films with at least more than 200 nm in film thickness. Examples for *anisotropic strain*: (b) Substrate supported free-standing metal oxide film membrane. In latter the membranes start to buckle upon the strain from the interface increasing locally the strain in the buckled film part. Changes in the point defect concentrations under strained membranes are reported [29,30,72]. (c) An anisotropic strain field occurs through lattice misfit as in the case for i.e. epixatially grown heterolayer interfaces of metal oxides films of different materials. Changes in the electric transport are reported, see i.e. recent review for details [76].
This graph c is adapted according to Korte et al. [131].

technique to determine the lattice strain is to measure the overall off-centering of the long-range cationic order through X-ray diffraction, see i.e. Brown and Lukens [40], or recent advanced descriptions by Stukowski [43] or Forest and Sievert [44]. In the case of X-ray diffraction Williamson–Hall plots [45] are an established technique in which the full width of half maxima of X-ray peaks are related to their diffraction angles through the Scherrer and Wilson equation [37,38]. Advantageous of lattice strain determination through X-ray diffraction is the common equipment access for laboratories, and the possibility to study strain evolvement versus temperature and time through in-situ heating. It may be considered as a drawback that the here measured strains describe mostly the off-centered cationic disorder for a metal oxide thin film, and specific strain-related changes in the anionic lattice are not directly measurable. One may also consider to study strain through the anisotropic Raman peak profile fits of F_{2g} lattice vibrations such as the O–Ce–O or O–Zr–O stretching modes for cubic symmetries, see i.e. Ref. [46]. Neutron diffraction is the most elegant experimental technique to investigate lattice strain and correlate these to changes in the anionic and cationic lattice order for a metal oxide relative to its processing history. However, literature examples for lattice strain measurements on zirconia- and ceria-based metal oxide thin films based on neutron diffraction are still missing.

It is important to note that the interaction of ionic diffusion, changes in elastic properties, phases and also interfacial-strain was discussed earlier for interfaces in polycrystalline bulk ceramics i.e. by the group of Schmalzried and Backhaus-Ricoult [47–50]. However, the overall thin film processing-related strain fields and their implications on ionic motion for polycrystalline metal oxide films are not discussed. Till now most of the authors attribute the differences in the electric characteristics of ionic conducting thin films to variations in the grain size through changes in the grain–grain boundary volume ratio [51–56]. I.e. ceria-based thin films show differences up to 30% in their activation energy of conductivity, several different orders of magnitude in their electrolytic domain boundary and up to one order of magnitude difference in total conductivity depending on their processing [57,58]. In contrast, zero-strained microcrystalline ceria bulk ceramics processed through calcination and sintering reveal only a minor processing dependence of the electric properties [30,59]. It is interesting to note that similarly broad differences in ionic transport are also reported for perovskites, zirconia- and titania-based materials for thin film processing [11,53,54,60,61]. However, the link between grain size, lattice-strain state and ionic transport remains unclear for the given examples of state-of-the-art ionic conducting oxide thin films.

Even though reports on the atomistic disorder and *lattice-strain* of polycrystalline ionic conducting thin films and their processing history are rare (Fig. 1a), one may learn from literature on the interplay of *strain* fields and ionic transport on *epitaxial heterolayer interfaces* (Fig. 1b) and *free-standing polycrystalline thin film membranes* (Fig. 1c). The major difference between processing related lattice-strain in polycrystalline ceramic film and strain at heterolayer interfaces or in free-standing membranes is in the strain tensor components and its consequence in giving isotropic or anisotropic strain fields, see Ref. [62] for details. For a polycrystalline film an overall total isotropic strain is measured through experimental techniques, which comprises all local strain fields and general off-centering of ions. In contrast strains at heterolayer interfaces and in free-standing film membranes are always anisotropic; these anisotropic strains are clearly tensile or compressive.

Examples for anisotropic strain in literature: (i.) Ceramic *heterolayer interfaces* consist of two different materials coherently grown thin films of 1–60 nm single film thickness [63]. The strain is anisotropic and directed through the heterolayer interface because it results from the lattice misfit at the interface of the two coherently grown films. State-of-the-art material systems for heterolayers are yttria-stabilized zirconia (YSZ)/$SrTiO_3$[63,64], YSZ/Lan_2O_3 (Lan = Lu, Sc, or Y) [65], YSZ/gadolinia-doped ceria (CGO) [66,67] or CGO/$SrTiO_3$[68,69]. The choice of the heterolayer material decides whether a compressive or tensile strain occurs. The strongest increase of ionic conductivity, namely by eight orders of magnitude, have been reported for 7% interface strain in coherently grown $SrTiO_3$–YSZ–$SrTiO_3$ heterolayers of 1 to 10 nm thickness by Garcia-Barriocanal in 2008 [64]. The authors emphasize that the tensile strain leads to a highly disordered oxygen plane at the interface of the films with superior ionic conductivity compared to classical ionic transport in sintered microcrystalline bulk ceramics. Cavallaro et al. contributed in 2010 that the interface orientation of YSZ and $SrTiO_3$ epitaxial films plays a crucial rule in the overall conductivity enhancement [70]. Sillassen et al. reported three order of magnitude conductivity increase for YSZ–$SrTiO_3$ heterolayers due to a combination of misfit dislocation and elastic strains [71]. Throughout the last two years high strains that improved the electrical conduction through heterolayers were proven to be promising, even though the reported values of Garcia-Barriocanal, Cavallaro et al. and Sillassen et al. could not be reproduced so far by other groups. Nevertheless, it has been confirmed by several authors that up to 4% strain can be realized, leading to an increase of ionic conductivity by at least one to two orders of magnitude for heterolayers based on YSZ [63,65], and CGO [68,69]. (ii.) A very recent field, to observe the impact of stress on anisotropic-strain and ionic diffusion are *free-standing polycrystalline thin film membranes*. In these experiments ceramic membranes are free-etched on a Si-wafer substrate and subjected to thermal heat treatments. Due to the thermal expansion mismatch between the substrate, i.e. Si, and the ceramic material the membranes start to buckle (compressive stress) or tighten (tensile stress) depending upon temperature. The membrane reacts on the external stress with anisotropic strain, whereby the unit cells of the membrane film close to the substrate vary towards those near to the air interface. Depending on the thermal expansion mismatch of substrate and ceramic thin film material a compressive or tensile strain situation may be present. Lubomirsky and co-workers reported as pioneers in the field that opposing or relaxing stress on the free-standing distorted lattices of ionic conducting metal oxide thin film membranes affects the migration of the oxygen ions named as “chemical strain effect” [29–32]. Membranes can relax the internal strain through point defect association–dissociations such as the formation and dissociation of gadolinia–oxygen vacancy clusters in $Ce_{0.8}Gd_{0.2}O_{1.9-x}$ with respect to temperature and time [27,31,72,73]. Recently, the first studies were published on the strain values of free-standing zirconia-based thin film membranes on Si-wafer substrates [74,75]. In all of these studies vacuum-based thin film techniques such as sputtering or PLD were used. The impact of the initial thin film processing method choice on the anisotropic strain characteristics of the membranes has not been investigated so far.

In view of applications as functional ionic conducting electroceramic layers in Si-wafer based electroceramic devices *tensile or compressive strained heterolayers* or *stressed thin film membranes* are highly encouraging as these are oxide systems with high ionic conductivity of one to two orders of magnitude [11,24,79]. However, these have common drawbacks for realization of fast ionic conducting layers: The strain fields are always directed and anisotropic. Fast ionic diffusion pathways will always be perpendicular to the heterolayer surfaces or to the surface of a free-etched membrane. This strongly limits the design flexibility of Si-based electroceramic devices, as only cross-ionic conductivity of the films in the device may be used during operation. Thermal long-term stability of strained heterolayer interfaces and free-standing film membranes is critical in these fields: in a recent report it was pointed out that interdiffusion at epitaxial $SrTiO_3$/YSZ heterolayers affects the strain and electric characteristics [70]. Moreover, “chemical strain” in membranes led to stress compensation by reordering and clustering of point defects, and thereby, unstable material systems.

Polycrystalline single thin films of more than 200 nm in film thickness offer a unique situation to study the interplay of structural disorder and lattice strain for ionic diffusion with respect to film processing. *Lattice strain* can be investigated besides the impact of other conventional microstructure characteristics such as grain size, amount of interfaces or degree of crystallinity. In contrast to strained heterolayer interfaces the strain fields in polycrystalline thin films are isotropic extending over the whole thin films' grain–grain boundary microstructures. The overall strained volume is larger for the polycrystalline films compared to the interface restricted compressive or tensile strain i.e. in heterolayer interfaces with single film units of conventionally some nm in thickness. Despite the potential of lattice-strained polycrystalline ceramic thin films for fast ionic diffusion pathways it remains unclear how strongly the actual lattice strain levels can be affected through thin film processing and annealing. Knowledge on experimentally determined strain values for standard ionic conducting thin film materials is missing in current literature. Their atomistic changes on anionic and cationic positions, their local ionic bond strength and implications on oxygen vacancy diffusion relative to strain and processing history are unknown for thin films.

This present manuscript investigates the interplay of the ionic conductivity and *lattice-strain* with respect to ceramic thin film processing on base of current literature. For this, a state-of-the-art ionic conducting material in air namely gadolinia-doped ceria is selected as a case example. Only, those reported papers that are focused on minimum measured microstructural characteristics and electric conductivity or ionic diffusion measurements are considered. $Ce_{0.8}Gd_{0.2}O_{1.9-x}$ thin films are focused as these are *single phase* and the *doping level is high*.

The *single phase* nature of ceria-based material is perfect for these fundamental considerations as the material cannot compensate for low lattice packaging densities or high internal strains by phase change. The only option for this material to compensate high strain energies is through bond braking, defect reordering such as oxygen vacancy pair formations of hampered mobility, possibly leading to changes in non-stoichiometry. The contrast is the case for phase-polymorph zirconia-based materials: Kushima and Yildiz [80], Heiroth et al. [81,82] and Scherrer et al. [83] confirmed through modeling and experiments that YSZ thin films react upon lattice strains (>3%) with reordering of nearest neighbor cations and phase change between cubic and t″. It can be concluded that firstly, single phase material such as ceria-based ones cannot react with phase transformation for high strains or disorder levels. Secondly, *high doping levels* of 20 mol% gadolinia in ceria result in high overall ionic strengths of the material system. Through the high dopant concentration enough oxygen vacancies are introduced into the ceria lattice to assure a predominant ionic conductivity in air up to temperatures of 1000 °C [57,59]. It was confirmed experimentally by Birringer and co-workers that space charges do not affect the total conductivity for gadolinia doping levels larger than 2 mol% in ceria [84,85]. This is in agreement with the space charge studies of Maier and co-workers for doped and pure ceria [86–90].

In all previously outlined literature examples of strain and ionic diffusion (Fig. 1) artifacts such as the *substrate influence* need to be critically discussed. It is known that for small film thicknesses especially in the range of less than 100 nm: (i.) the substrate may oppose additional anisotropic strain affecting the electric properties of a film, see i.e. recent review by Santiso and Burriel [76], (ii.) short circuiting through the substrate may take place modifying the effectively measured electric conduction of a film, see i.e. recent publication by Kim and co-workers from the KIST micro-Solid Oxide Fuel Cell team [77], and (iii.) or chemical inter-diffusion between the substrate and a film may change the original thin film composition, its strain and electric conduction [78]. Therefore, only those papers are discussed where the thin films reveal at a minimum 200 nm in film thickness, and, strain and electric measurements were undertaken in a temperature regime where the substrate (i.e. sapphire or MgO) does not show interdiffusion with the ceria-based thin film.

It is also important to note that the lattice strains of the films compared through this manuscript were conventionally determined through X-ray diffraction through Williamson–Hall plots [45] as described earlier in this chapter. This signifies that predominantly the cationic displacement fields through grain–grain boundary are experimentally probed in these films.

Finally, it can be concluded that changes in the ionic conduction of $Ce_{0.8}Gd_{0.2}O_{1.9-x}$ thin films are classified in this review as pure function of structural differences related to thin film processing and annealing history. Neither phase changes, nor space charges, nor substrate influence for too small metal oxide film thicknesses, nor differences in strain determination techniques are supposed to affect the here reported ionic conduction characteristics of the material in air.

This manuscript investigates the impact of processing on lattice strain and ionic transport of metal oxide thin films on the material example of gadolinia-doped ceria ($Ce_{0.8}Gd_{0.2}O_{1.9-x}$, CGO) in air.

In the first introductory part, literature on the impact of strain on ionic conduction of electroceramic thin films is reviewed, the definition of lattice strain and its experimental determination is presented, working hypothesis why thin film processing can affect lattice strain states and ionic migration is raised, and boundary conditions for the discussion of own experimental data relative to literature are set for this study. The second part reviews the impact of the original thin film method choice and processing on the thin film microstructure, chemistry and lattice packing. In the third part, a well known working hypothesis in literature that the electric characteristic scale as a function of “grain size” through variation of the grain to grain boundary volume is discussed. In the fourth part, the role of processing related disorder on electric characteristics is reported. *Lattice-strain* is proposed as a new measure to account for the differences in processing related changes in local ionic bond strength of the crystal lattices. First summary on quantitative lattice strain changes relative to processing method and history is given relative to literature. Point defects, different degrees of crystallinity and changes in crystallographic density are discussed. In the fifth part the impact of lattice strain on ionic diffusivity for polycrystalline thin films is discussed. The sixth and penultimate part focused on initial reports relating the local chemistry over grain–grain boundary to the lattice strain state of CGO thin films. Finally, engineering guidelines for processing of high ionic conducting thin films through lattice-strain for Si-based electroceramic devices are given in the concluding remarks.

2. The choice in ceramic thin film method: impact on microstructure

The techniques in the preparation of metal oxide thin films can be separated into two major groups, namely: the *vacuum-based techniques* in which the thin films are deposited from a sintered pellet target, and the *precipitation-based techniques* based on organic or aqueous solvents. The major differences between both classes of these thin film processing techniques are the degree of disorder introduced during deposition. Atoms are deposited directly from an ablated sintered pellet target under reducing vacuum conditions in the case of vacuum-based techniques, whereas oxide films are deposited over a pyrolysis reaction in case of most precipitation-based technique. As a result mostly crystalline and often slightly reduced films are deposited for the vacuum-based techniques, and purely amorphous and oxidized films often with hydroxyl- and carboxyl-residuals are deposited for precipitation-based techniques [91].

Literature reports on processing of gadolinia-doped ceria thin films through *vacuum-based techniques* like physical vapor deposition [92], pulsed laser deposition (PLD) [86,93] or RF-sputtering [94–97], as well as *precipitation-based techniques* such as chemical vapor deposition [98,99], atomic layer deposition [100,101], spray pyrolyis

[91,102,103], sol–gel [54,104,105] or flame spraying [106]. Typical film thicknesses of the thin films are between 200 and 500 nm and the films are mostly deposited on electrically insulating substrates such as sapphire or MgO for future electric characterization [13,79,107]. For example, the microstructures of $Ce_{0.8}Gd_{0.2}O_{1.9-x}$ thin films processed through vacuum- and precipitation-based techniques are displayed in Fig. 2.

Precipitation-processed thin films grown by flame spray and spray pyrolysis are presented in Fig. 2a [106] and b, respectively. Both, films were originally deposited in X-ray amorphous state and were crystallized to full crystallinity through post-annealing at about 1000 °C. The thin films show isotropically grown grains of no preferred orientation embedded in a dense thin film matrix with sharp grain boundaries and grains around 80 nm in average grain size. In contrast, the vacuum-based thin film examples processed by PLD, Fig. 1c [108] and d [109] reveals a preferred growth direction of the grains perpendicular to the substrate. Typical column widths of the PLD $Ce_{0.8}Gd_{0.2}O_{1.9-x}$ thin films are around 80–100 nm. Latter columns are slightly separated by voids, see for example the PLD film processed by Joo and Choi [109] (Fig. 2d). The difference to isotropic grains of precipitation-based microstructures such as the spray pyrolysis thin film in Fig. 2b can be recognized in the in-plane views of the dense microstructures with no voids at the triple points of the grains.

The selected microstructure examples illustrate the high variety in crystallization and grain growth ranging from isocrystalline to columnar microstructures for a single material, gadolinia-doped ceria, with respect to processing method choice. The impact of film processing on microstructure can be studied in the field of micro-Solid Oxide Fuel Cell membranes. These Si-wafer based electroceramic devices rely on gas-tight and ionic conducting electrolyte thin films. Until now, only the fuel cells based on precipitation-based techniques such as atomic layer deposition (ALD) [4,8,110], or combinations of a bilayer structure through a precipitation-based spray pyrolysis and a vacuum-based PLD film [6] resulted in theoretical open circuit voltage and promising power-output. Microstructures of single vacuum-processed electrolyte films through sputtering [111,112] or PLD [113,114] showed always columns leading to gas-leakage and insufficient fuel cell performance. The initial choice in thin film processing is of relevance for the ionic bond strengths and packaging density of the grains, their connectivity and growth, all of which requires careful consideration for ionic conductors.

In Table 1, the film thicknesses, characteristic grain shapes, average grain size, degree of crystallinity and lattice strain are summarized with respect to measured electric conduction properties for $Ce_{0.8}Gd_{0.2}O_{1.9-x}$ thin films on the basis of literature. Concerning the microstructures it can be noted that most authors characterize the grain size of the thin films, but do not report on the degree of crystallinity of the thin films. The thin films may exhibit besides crystalline also amorphous residual phases which can affect the ionic diffusion pathways of the material. First reports on measured lattice strain data exist for $Ce_{0.8}Gd_{0.2}O_{1.9-x}$ thin films from Kargeorgakis et al. [106], Suzuki et al. [115] and Rupp et al. [116].

The impact of grain size, lattice strain and the degree of crystallinity on the ionic conductivity in air is discussed in the following parts.

3. Grain size effects in nanocrystalline thin films — an approach to explain ionic diffusion differences in thin films?

In literature, the *grain size* is often discussed as a size-effect to affect the ionic conductivity of ceria-based materials [51,53,117,118]. Especially, in thin films the average grain size is often only one tenth or a third of the overall film thickness, and grain boundary

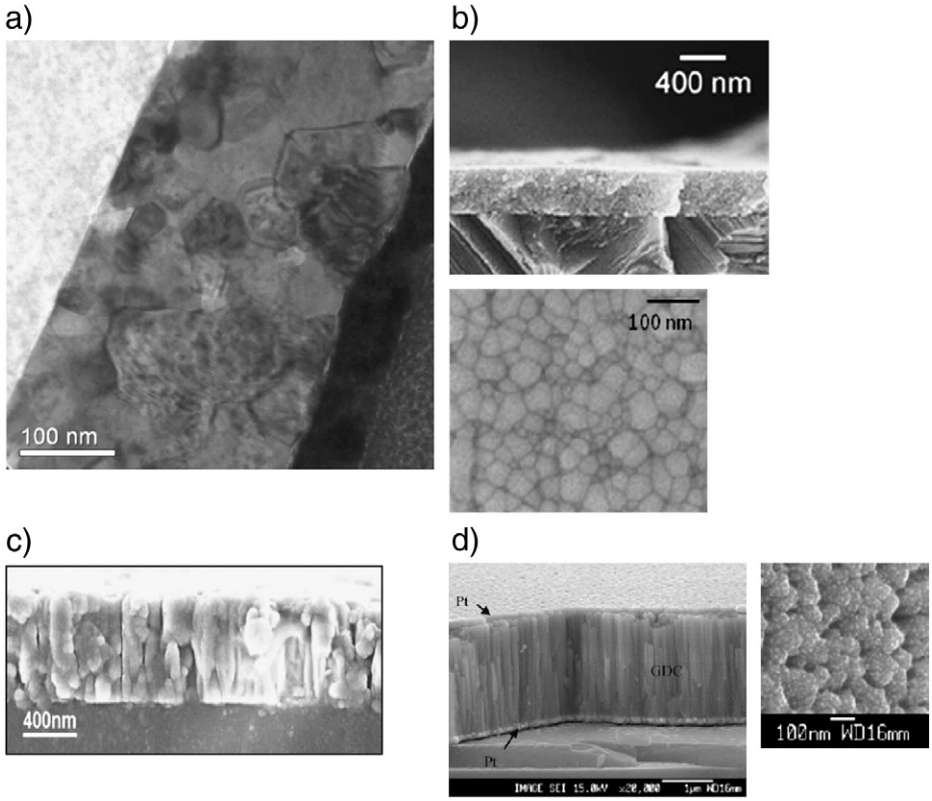

Fig. 2. Literature examples on the microstructures of $Ce_{0.8}Gd_{0.2}O_{1.9-x}$ thin films processed through precipitation- and vacuum-based thin film methods. (a) TEM bright-field cross-section of a precipitation-processed flame spray film, (b) SEM cross-section and top-view of a precipitation-processed spray pyrolysis film, (c) SEM cross-section of a vacuum-processed PLD film, (d) SEM cross-section and top-view of a vacuum-processed PLD film. Please note that all thin film examples reveal film thicknesses clearly larger than 200 nm. Reprinted with permission from Wiley for images (a) and (c) [106,108], personal data of the author J.L.M. Rupp for images (b), reprinted with permission from Elsevier for (d) [109].

Table 1
Literature review on $Ce_{0.8}Gd_{0.2}O_{1.9-x}$ thin films with respect to their processing, microstructure characteristics and electric conduction properties. The abbreviation PLD denotes the thin film deposition method of pulsed-laser-deposition.

Thin film microstructure						Thin film electric properties			Ref.
Thin film processing method	Film thickness (nm)	Grain growth	Average grain size (nm)	Degree of crystallinity (%)	Lattice strain (%)	Electrical conductivity at 500 °C (S/m)	Electrical conductivity activation energy (eV)	Oxygen partial pressure of EDB at 700 °C (atm)	
PLD	500–1800	Columnar	40–90 (column width)	–	–	0.0002	0.86	10^{-19}	[109]
	200		40–80 (column width)			0.0001–0.0002	0.74–0.86	10^{-19}	[124]
	400	Isotropic	46			0.06	0.8	–	[58]
			55			0.05	0.88	10^{-17}	[57,58]
			75			0.04	1.05	–	[58]
RF-magnetron sputtering	100		80			0.0003	0.95–1.05		[107]
Sol–gel	350	Isotopic	11	100	1	0.01	1.05	–	[115]
			15–20		0.22		1.2		
			36		0.015		1.35	10^{-14}	
Flame spray	400–500		20		0.16	0.1	0.76	–	[106]
			25		0.13	0.06	0.85		
			35		0.075	0.04	1.1		
Spray pyrolysis	300		29	100	1.2	0.09	0.77		[58,116]
			59		0.9	0.06	0.85		
			76		0.2	0.06	1.04	10^{-16}	[57,58,116]

volume increases relative to the grain volume with decreasing grain size. Adapted from Christie and Berkel's "Brick layer model" for bulk ceramics from the 90s [119] it is assumed that a decrease in the grain size in an ionic conducting thin film would systematically lead to an increase in grain boundary conductivity, i.e. discussions by Suzuki, Kosacki and Anderson on ceria and zirconia [54,55,115,120]. The authors reported that decreasing the overall grain size of $Ce_{0.8}Gd_{0.2}O_{1.9-x}$ spin coated thin films from 36 to 11 nm in average decreased the activation energy of conductivity in air from 1.3 to 1 eV while increasing the ionic conductivity by one order of magnitude, see Fig. 3a. This tendency was reported to be independent of the concentration of the dopant. Investigations on PLD and spray pyrolysis $Ce_{0.8}Gd_{0.2}O_{1.9-x}$ thin films confirmed similar qualitative findings. Decreasing the grain size from around 80 to 40 nm led to a decrease in the activation energy of 1 to 0.8 eV. The ionic conductivity increased around one order of magnitude, see Fig. 3b [58]. It is to be noted that the examples selected from literature, see Fig. 3, compare a precipitation-processed thin film (spin coating) to a vacuum-processed (PLD) thin film. This comparison reveals that processing related chemical impurities are unlikely to cause the observed decrease in activation energy with increasing grain size of the films. Two completely different processing approaches lead to a similar qualitative finding. Nevertheless, none of the studies clarified the reasons for the change in electric properties beyond speculations on grain size effects.

Literature-reported activation energies of ionic conductivity (air) are summarized with respect to average grain size and thin film processing method for $Ce_{0.8}Gd_{0.2}O_{1.9-x}$ thin films in Fig. 4. All films analyzed revealed film thicknesses of 200 to 500 nm, and electric measurements were taken out in air. Systematic studies varying the average grain size through different temperature annealing prior to the electric measurements are indicated with dashed lines. The degree of crystallinity is determined as fully crystalline in case of the spray pyrolyzed and fame sprayed films [58,106,121]. However, it remains unknown for all other references, see Table 1.

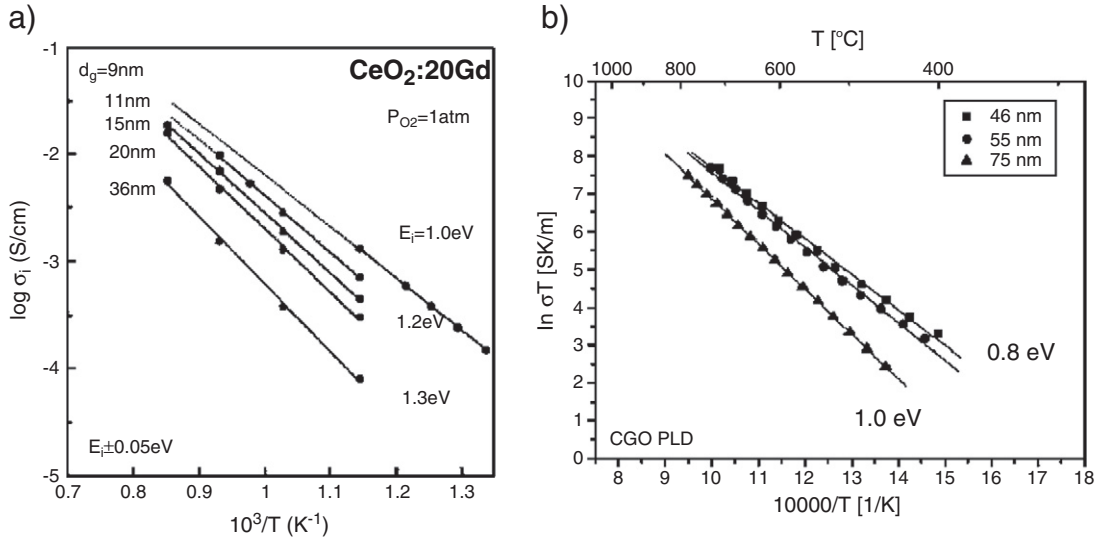

Fig. 3. Arrhenius diagrams of ionic conductivity of $Ce_{0.8}Gd_{0.2}O_{1.9-x}$ thin films with respect to average grain size and temperature. The thin films were processed by (a) the precipitation-based method of spin coating and (b) by the vacuum-based method of pulsed laser deposition. Please note that the average grain sizes of the films are indicated in nm for (a) left side besides the electric data, and for (b) in the legend. Both films were larger than 350 nm in total film thickness, see Table 1 for further microstructural details. Data were reprinted with permission from Elsevier for (a) [115] and (b) [58].

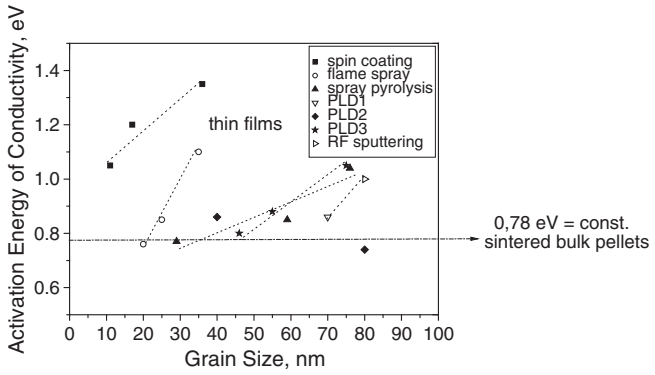

Fig. 4. Literature review: activation energy of electric conductivity in air of $Ce_{0.8}Gd_{0.2}O_{1.9-x}$ thin films with respect to grain size and thin film processing route. State-of-the-art $Ce_{0.8}Gd_{0.2}O_{1.9-x}$ sintered bulk ceramic pellets reveal a constant and grain size independent activation energy of 0.78 eV in most cases [132–134]. Please note that all thin film examples reveal film thicknesses clearly larger than 200 nm, see Table 1. Data of electric conductivity refer for spin coating processed films to Suzuki et al. [115], Kargeorgakis et al. [106], Rupp et al. [58], PLD1 to Joo et al. [109], PLD2 to Chen et al. [124], PLD3 to Rupp et al. [58] and RF sputtering to Chipdelli et al. [107]. The abbreviation PLD denotes the thin film deposition method of pulsed-laser-deposition.

The following conclusions can be drawn on the basis of this review for $Ce_{0.8}Gd_{0.2}O_{1.9-x}$ thin films (Fig. 4):

1. Studies describe that the activation energy reduces with decreasing average grain size of a thin film. This tendency holds for differently processed thin film-grain size studies, vacuum- as well as precipitation film processing. Within a study with one choice of thin film processing method up to Δ0.3 eV scatter in activation energy of conductivity are reported for a total change in the average grain size of Δ30 to Δ50 nm.
2. Comparing the different studies it remains clear that *similar grain sizes do not result in similar electric characteristics*. For example the activation energy of ionic conductivity scatters between 0.8 and 1.4 eV for an average grain size of 40 nm with respect to the film processing method choice. Consequently, differences up to Δ0.5 eV in activation energy of conductivity exist dependent on the thin film processing method chosen for a similar grain size in literature. The smaller the grain size the larger becomes the scatter in the reported activation energies of ionic conductivity.
3. The scatter in the activation energies of ionic conductivity is not even method specific. Precipitation-based films do not show comparable electric characteristics for different processing methods, e.g., spray pyrolysis, flame spray, and spin-coating. This is also in agreement with findings for vacuum-processed films.
4. $Ce_{0.8}Gd_{0.2}O_{1.9-x}$ sintered bulk ceramics reveal typical activation energies of 0.78 ± 0.05 eV [59,122,123], whereas in this review we find that thin films show activation energies of 1.1 ± 0.3 eV. The scatter for the electric conduction properties of the material $Ce_{0.8}Gd_{0.2}O_{1.9-x}$ is to be valued as high for thin film processing, and electric conduction of the material has to be considered to vary by up to one order of magnitude dependent on the processing method.

In Table 1, the electrolytic domain boundaries (EDBs) are reviewed with respect to thin film processing PLD [57,109,124], sol–gel [115] and spray pyrolysis [57] for $Ce_{0.8}Gd_{0.2}O_{1.9-x}$ films. All reports agree that a predominant ionic conduction takes place in the material for electric measurements in air. The EDBs vary method specifically from 10^{-14} to 10^{-19} atm for 700 °C, and reflect the high variance in electric transport characteristics for thin films dependent on the chosen film processing method. According to Mogensen et al. [59] and Eguchi and co-workers [122] the EDB at 700 °C remains at 10^{-21} atm independent on the processing of sintered bulk ceramics.

It can be concluded on the basis of this literature review that the broad changes in activation energy of conductivity in air represent predominantly changes in the ionic diffusion characteristics of thin films. It is not possible to reasonably ascribe the scatter in activation energy of 1.1 ± 0.3 eV to pure scaling laws such as the commonly named "grain size effect". Similar grain sizes do not result in comparable electric characteristics for the material.

The ionic conductivity of ceramic thin films such as the given example of $Ce_{0.8}Gd_{0.2}O_{1.9-x}$ (air) is a strong function of the thin film processing.

It is proposed to take into account changes in the local ordering of atoms after thin film processing and annealing and differences in the ionic bond strengths and varying defect levels for discussion of ionic conductivity in thin films. In the following, *lattice-strain* is discussed as an additional microstructural parameter to account for this besides grain size and crystallinity.

4. Characterizing disorder in thin films: lattice-strain as a measure

The choice in processing method and thermal history of a ceramic thin film affects the degree of crystallinity, the overall packing density, and internal ordering of atoms. The resulting displacement fields can be classified in terms of the lattice strain. Please note that the different possibilities to measure lattice strain on thin films were discussed in the introductory part (Section 1) of this manuscript.

It is reported in the literature that decreasing the grain size of a thin film results in an increase of the overall lattice strain (microstrain). In Fig. 5, the evolution of strain with respect to grain size is plotted for spin coated ceria-based thin films with respect to doping [115,120]. Decreasing the average grain size from 100 to around 10 nm increases the lattice strain of the thin films by one order of magnitude. In the given study the strain was determined via the Scherrer and Willson equation analysis of XRD data [37,38]. Recent Raman investigations confirmed that high lattice strains determined by XRD are clearly correlated to widened ionic bond length and larger amounts of defects on the example of sprayed undoped ceria thin films [46]. The widening of ionic bond length was measurable through a red shift and the increased defect concentrations through the asymmetry of the Raman active F′ mode reflecting the Ce–O(8) bond units.

Reported actual lattice strain values vary between 7% [116] and 0% depending on the thin film processing choice and the degree of crystallinity of $Ce_{0.8}Gd_{0.2}O_{1.9-x}$ thin films, see Table 1. The strain of $Ce_{0.8}Gd_{0.2}O_{1.9-x}$ thin films varies during the crystallization, as well as for differently annealed fully crystalline states. In Fig. 6, examples of ceria-based spray pyrolysis thin films are given in which the degree

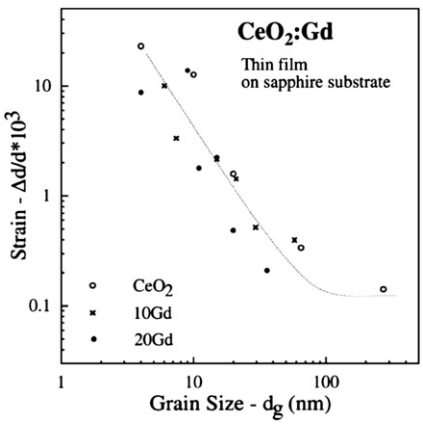

Fig. 5. Evolvement of strain with respect to grain size in sol–gel gadolinia-doped and undoped thin film. The thin film was 350 nm in film thickness according to the authors [115].
Data were reprinted with permission from Elsevier for (a) [115].

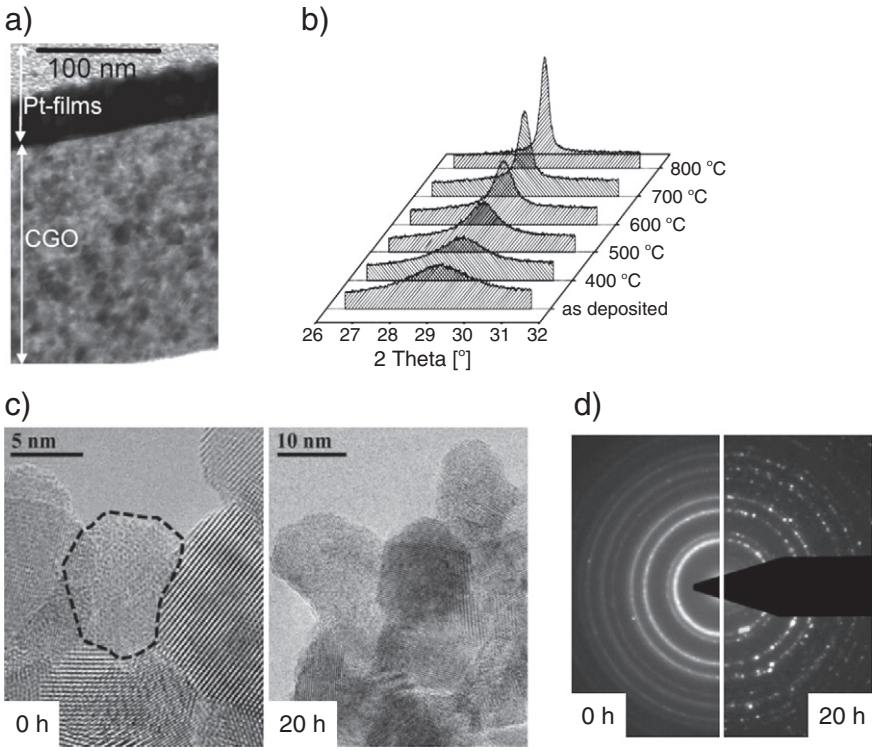

Fig. 6. The given literature example on a precipitation-processed thin films deposited by spray pyrolysis reveals the transition from amorphous to biphasic amorphous–crystalline to finally full crystallinity during crystallization of an originally amorphous ceria-based thin film. (a) STEM image of a FIB cut cross-section of a $Ce_{0.8}Gd_{0.2}O_{1.9-x}$ thin film (annealed for 0 h at 600 °C) [135], (b) evolvement of the XRD (100) peak during crystallization for a CeO_{2-x} thin film with respect to post-annealing [125], (c) STEM analysis of the grains of a CeO_{2-x} thin film for an isothermal dwell at 600 °C for 0 and 20 h [125]. Lattice plane ordering proceeds with increasing dwell time [125], (d) Corresponding TEM diffraction patterns to (c) [125]. Please note that all thin film examples reveal film thicknesses clearly larger than 300 nm, see Table 1.

of crystallinity varies with respect to thermal history after film deposition. In the given examples the crystallization is monitored through in-situ XRD and accompanying TEM studies of the grains in ceria-based films. In the XRD the ongoing crystallization may be followed over temperature through the peak sharpening of the (100) reflex of the cubic lattice from an amorphous halo. The STEM example shows the on-going atomic ordering in the bright field mode and corresponding diffraction pattern of single grains in the film for isothermal hold from biphasic amorphous–crystalline to full crystallinity of the films.

In Fig. 7, the evolvement of lattice strain is plotted over time and temperature during crystallization of $Ce_{0.8}Gd_{0.2}O_{1.9-x}$ spray pyrolysis and flame sprayed thin films. Grain size evolution is given as well to discuss the interplay of crystallization–strain–grain size evolvement for a thin film. The obtained data confirms again that a decrease in grain size is always accompanied by increased strain of the thin films. It is further shown that the residual strain values differ for equal post-annealing conditions, as these are processing method specific. For example strains of 7 and 0.4% are reported for a spray pyrolysis and flame sprayed film for similar chemistry at 600 °C. Interestingly, the strains of the films can always be fully relaxed to 0% by heating the thin films to temperatures above 1000 °C. In the temperature field between room temperature and 1000 °C the actual strain values are related to the thermal history (heating rates, isothermal holds, etc.). It was recently confirmed in the case of sprayed films that within this temperature range the material's crystallization is on-going in parallel to grain growth and strain reduction [121]. Biphasic amorphous–crystalline films relax during an isothermal hold in their lattice strain to a constant value following an exponential decay function [116]. Differential scanning calorimetry (DSC) studies confirmed that the relaxation times coincide with the transformation of these biphasic amorphous–crystalline microstructures to full crystallinity during an isothermal hold [121,125]. Grain growth follows on for the biphasic states through self-limited grain growth kinetics [116]. For temperatures high enough to assure full crystallinity through heating (usually above 1000 °C for ceria-based films) zero strain is measurable and conventional parabolic grain growth kinetics driven by the grains' curvatures prevail [116,125]. Recently, Time–Temperature-Transformation (TTT) diagrams were proposed to map and predict on the basis of experimental result the evolvement of the degree of crystallinity for metal oxide thin films such as ceria-based ionic conductors. The TTT-diagram of a $Ce_{0.8}Gd_{0.2}O_{1.9-x}$ processed spray pyrolyzed thin film is displayed exemplarily in Fig. 8. The crystallization rates of the material and best thermal processing routes to assure a specific degree of crystallinity can be determined with respect to temperature and time through the isocrystalline lines as indicated in the TTT diagram. Details on establishing experimentally TTT diagrams for metal oxide thin films are reported in Ref. [121].

On the basis of these TTT-diagrams different lattice strain states can be defined for thin films through isothermal dwells for times long enough to assure full crystallinity. An important side remark is that the strong changes in strain during crystallization mirror the on-going strong changes in ionic bond strengths in a dense solid state film. The evolution of ionic conductivity is discussed for fully crystalline thin films with different levels of lattice strain in the following part of this manuscript.

5. Lattice strain and ionic diffusion in fully crystalline thin films

On the basis of the Arrhenius diagrams of ionic conductivity in air the activation energies for CGO thin films were extracted, and compared to measured lattice strain through XRD, see Fig. 9. For this, studies were chosen in which the ionic conductivity was measured at lower temperature than a previous isothermal annealing step at which full crystallinity and a constant lattice strain value was established. Only precipitation-based thin films made by spin-

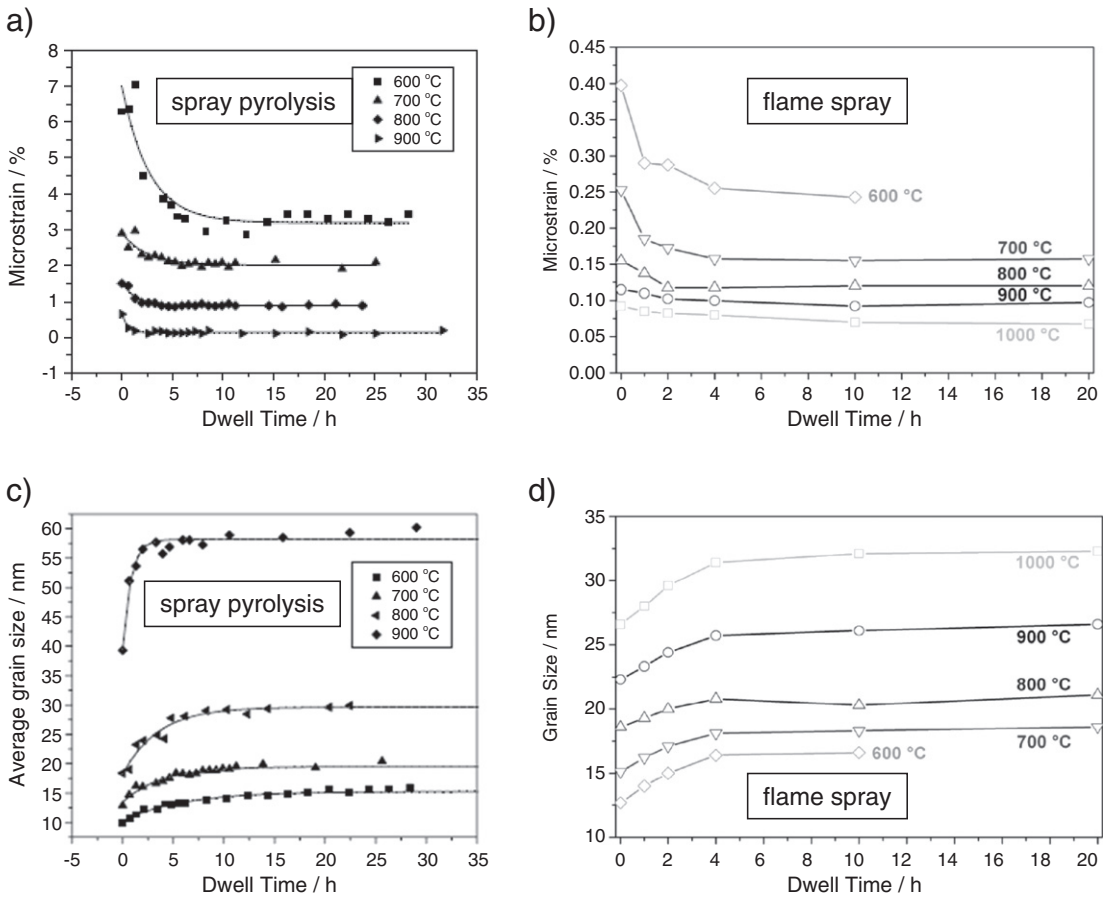

Fig. 7. Evolvement of strain and average grain size of $Ce_{0.8}Gd_{0.2}O_{1.9-x}$ thin films with respect to temperature and time for the precipitation-based processing methods: (a, c) spray pyrolysis [116] and (b, d) flame spray [106]. Please note that all thin film examples reveal film thicknesses clearly larger than 300 nm, see Table 1.
Data were reprinted with permission from Elsevier for (a, c) and from Wiley for (b, d).

coating, flame spray and spray pyrolysis can be compared since strain data on vacuum-processed films are currently missing in literature.

The following conclusions can be derived for the ionic diffusion measured in air of CGO thin films:

(i.) Decreasing the strain increases the overall activation energy of ionic conductivity independent of thin film method. Comparison of the ionic conductivity for 500 °C reveals that high strains of the material always correlate to high ionic conductivities of the material in air. This signifies that the more distorted the cubic lattice of the ceria-based thin film, the more facilitated is the ionic diffusion.

(ii.) Extrapolation of the activation energies to 0.01% of strain in the material results in similar high activation energies around 1.4–1.45 eV independent of thin film processing route. A similar tendency may be seen in the total ionic conductivity comparing the spray pyrolysis and flame spray thin film. Here, the ionic conductivity would equal to 0.035 S/m at 500 °C for approximately 0.04% of strain.

(iii.) The total ionic conductivity in air varies for fully crystalline films of low strain values of 0.08 to 1%, up to one order of magnitude in its value. Data for biphasic or amorphous ceria-based thin films are almost inexistent in the literature up to now. However, on the basis of the first TTT-diagrams for the case of CGO spray pyrolyzed films, and available data on strain during time–temperature post-annealing it is to be predicted that ionic conductivity will change even more drastically for biphasic amorphous–crystalline, or amorphous films as these can tolerate higher lattice strains of up to 7% compared to the herein before fully discussed crystalline films. This again demonstrates how important the local change in space along the ionic migration path and the interatomic bond strength between the migrating oxygen and the nearest neighbor cation are.

The *lattice strain* represents a suitable measure to reflect the ionic bond environment of a thin film material and its characteristic processing-related amounts of defects. Ionic diffusion characteristics of a thin film can be correlated to the thin film characteristic lattice strain fields for full crystallinity. The lattice strain represents an important measure to account for changes in ionic conductivity due to processing-related differences in packing densities or local ionic bond strength differences besides common microstructural measures such as grain size. Grain size alone is not a suitable parameter to discuss processing-related differences in diffusion of ionic charge carriers for thin films. Therefore, lattice strain measurements are suggested as an additional and important argument to account for changes in ionic migration barriers for thin film processing.

6. Lattice Strain vs. local chemistry for fully crystalline thin films

An open question is whether the local chemistry over the grain–grain boundary interfaces of a fully crystalline film varies with respect to the lattice strain state. A highly strained crystal lattice reveals local differences in ionic bond strengths and the dopant distribution and oxygen vacancy concentrations over a grain can no longer be assumed to be homogeneous. Strain-related changes in the ionic bond strengths can have severe consequences for the crystal lattice such as oxygen migration barrier changes, the hampered or promoted

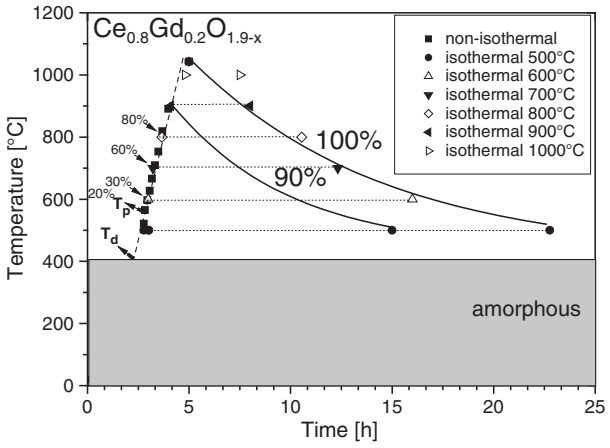

Fig. 8. Time–Temperature-Transformation (TTT)-diagrams for the originally amorphous $Ce_{0.8}Gd_{0.2}O_{1.9-x}$ thin films processed through spray pyrolysis. The plots display the thermokinetics of crystallization of the original amorphous thin films indicated by the degree of crystallinity in percentage. The important key temperatures for their crystallization are the deposition temperature (T_d) and the crystallization peak temperature (T_p). The C-type curves indicate the minimal heating rate required to reach the specific degree of crystallinity as given. These TTT diagrams can now be used to predict the crystallization degree of a thin film for pure isothermal or non-isothermal annealing, as well as their combination, and may give suitable guidance for the introduction of these thin films in electrochemical MEMS devices, e.g. as electrolytes in micro-Solid Oxide Fuel Cells. See Ref. [121] for details. Please note that all thin film examples reveal film thicknesses clearly larger than 300 nm, see Table 1.

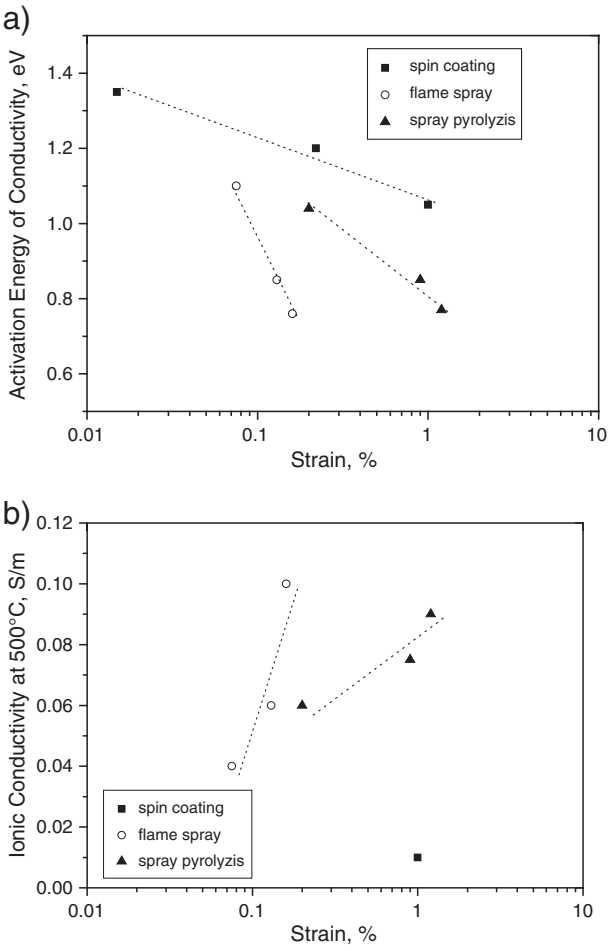

Fig. 9. Ionic conductivity characteristics with respect to lattice strain state and thin film processing of $Ce_{0.8}Gd_{0.2}O_{1.9-x}$ (air): (a) activation energy, and (b) ionic conductivity at 500 °C. Original data of electric conductivity and strain measurements refer for spin coating processed films to Suzuki et al. [115], Kargeorgakis et al. [106], and Rupp et al. [58,116]. Please note that all thin film examples reveal film thicknesses clearly larger than 300 nm, see Table 1.

formation of oxygen vacancies. As a consequence the cations can reduce or oxidize. Recent synchrotron diffraction studies on the impact of strain on SOFC cathodes of the $(La,Sr)CoO_{3-x}$ family concluded that chemical cation ordering associated to changes in oxygen vacancy concentration and cationic mobility can evolve upon strain [23]. First-principle calculations confirmed that tensile strain affects the defect chemistry such as the active formation of oxygen vacancies in these perovskite-systems [22]. Given these findings in the field of perovskites it is likely to assume that strains can affect the chemical anionic and cation concentration profiles of ceria-based thin films. First experimental studies have probed the chemical profiles through grain–grain boundaries of CGO thin films for a PLD vacuum-based film [126], and a flame sprayed precipitation-based thin film [106], are shown in Fig. 10. Both films had fully crystalline microstructures, whereby the vacuum-processed films revealed columnar microstructures, and the precipitation-based one grains of globular shape. In case of the flame sprayed film the lattice strain value was measured to be around 0.05% through XRD, for the PLD film the strain state is not reported. However, it can be assumed based on this literature review that the PLD film reveals a comparable strain state, see Fig. 9 and Table 1.

Comparison of the chemical profiles measured by line scans of either ELNES or EDX in STEM shows that the vacuum-processed film shows no variation of the chemical components of Ce^{3+}, Ce^{4+}, or Gd^{3+} over two columns of 50 nm in column width. In contrast, the precipitation-processed film exhibits an increased Ce^{3+} concentration in the grain boundary at constant Gd^{3+} level over the grain–grain boundary structure.

It can be concluded that the local chemistry at the grain–grain boundary of CGO thin films depends on the processing history and grain microstructure evolvement. What is unclear is whether these local differences in the reduction of the ceria can directly be attributed to the lattice strain. Till now there are no reports on the active atomistic changes of the cationic relative to the anionic ordering with respect to a thin films' lattice strain. Neutron diffraction experiments on ionic conducting thin films relative to their processing history may give important insights on the real atomistic changes under strain and their impact on ionic diffusion. Further, neutron diffraction experiments relative to changed grain–grain boundary ratios of a film may allow for first assumptions on the interplay of strain fields and chemical changes at real interfaces.

7. Concluding remarks

The importance of *lattice strain* for the electric conduction of state-of-the-art ionic conducting oxide thin films is discussed and proposals are given for the use of functional thin films in Si-wafer based electroceramic devices. Metal oxide thin films are deposited directly in dense form but differ in their atomic displacement fields over grain–grain boundaries and packing densities due to the thin film processing route and thermal history. The ionic diffusion is sensitive to the atomistic disorder and specific ionic bond strengths of a thin film. Lattice strain can alter the ionic migration barriers through changes in ionic bond strength between anions and cations, their reordering, or in an extreme case bond braking at high strain.

In this article the impact of thin film processing on the ionic conductivity is discussed through the *concept of anisotropic- and isotropic-strain fields*. To do so gadolinia-doped ceria thin films are focused as these are predominantly ionic conductors in air which remain always single phase even upon high strain fields. The role of thin film processing – vacuum vs. precipitation-based techniques – and post-annealing on the electric characteristics such as the ionic

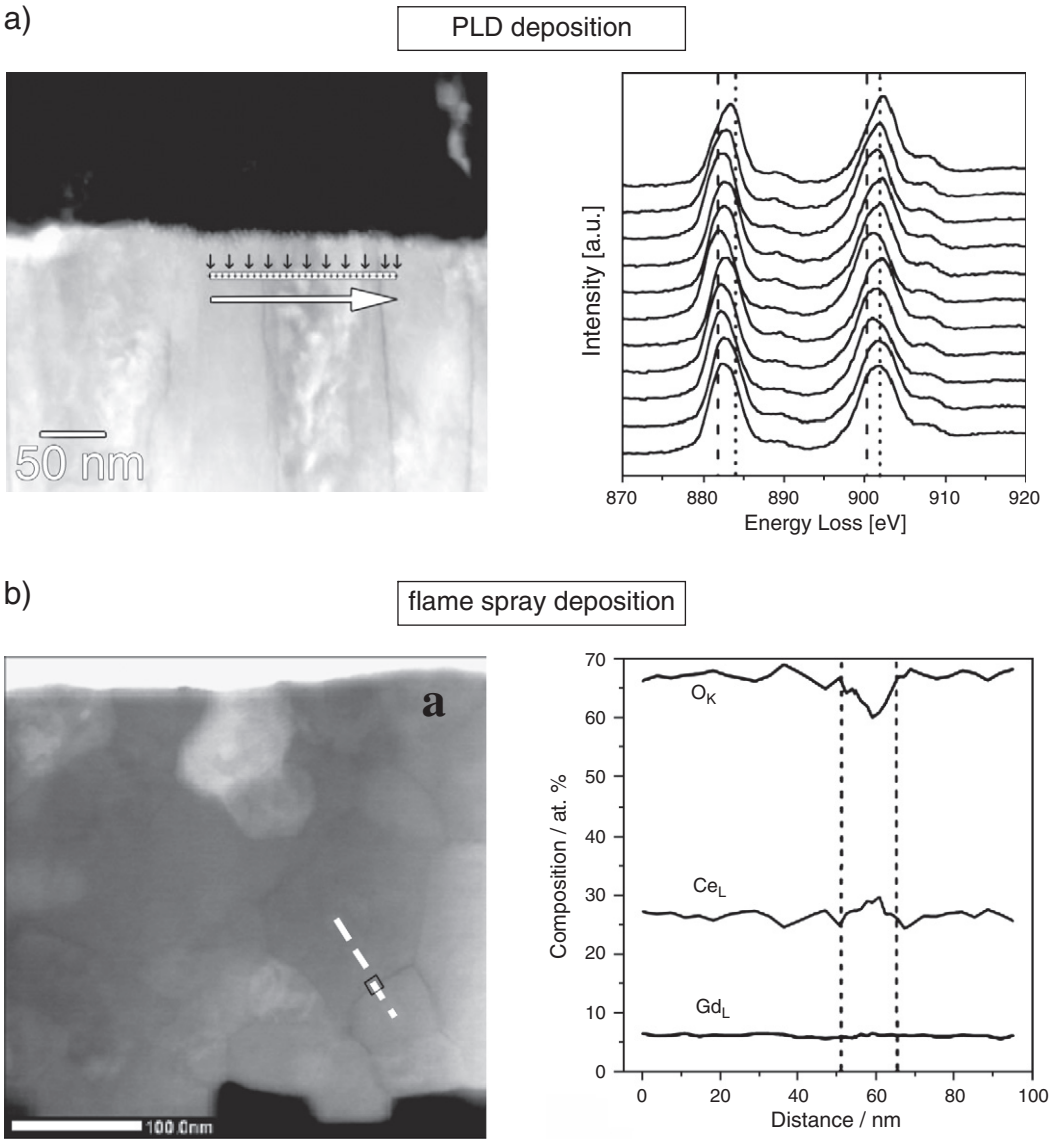

Fig. 10. STEM microstructures and chemical probing with respect to grain microstructure for a $Ce_{0.9}Gd_{0.1}O_{1.9-x}$ vacuum-based thin film processed by PLD and a $Ce_{0.8}Gd_{0.2}O_{1.9-x}$ precipitation-based thin film processed by flame spraying: (a) STEM-image of thin film microstructure, and ELNES positions presented by small arrows in the image relative to two adjacent columns. Ce^3/Ce^4 states are presented in the energy losses for a thin film deposited by PLD [126]. (b) STEM-image of thin film microstructure, and STEM EDX line-scan on the Ce_L, Gd_L and O_X profiles over a grain–grain boundary-grain structure for a thin film deposited by flame spraying [106]. Please note that all thin film examples reveal film thicknesses clearly larger than 300 nm, see Table 1.
Data were reprinted with permission from Elsevier for (a) and from Wiley for (b).

conductivity or the electrolytic domain boundary and on microstructural characteristics such as lattice strain, grain size and habitus, or the degree of crystallinity are reviewed. Only films with more than 200 nm in film thickness are considered in this paper to keep the impact of substrate on the overall films' lattice strain as low as considerable.

Literature review reveals that decreasing the grain size leads to increased lattice strain and measurable widening of the ionic bond lengths for a metal oxide thin film such as $Ce_{0.8}Gd_{0.2}O_{1.9-x}$. The actual percentage value of lattice strain is a thin film processing characteristic which varies also through the thermal annealing history and possible on-going crystallization processes. Therefore, lattice strain values determined for fully crystalline and biphasic amorphous–crystalline films require a clear demarcation. *Fully crystalline thin films* of $Ce_{0.8}Gd_{0.2}O_{1.9-x}$ differ up to 3.5% in lattice strain depending on the thin film method chosen and annealing temperature. The history of post-annealing is crucial for the actual lattice strain of the thin film. Low annealing temperatures dwells between 300 and 600 °C result in high lattice strains, whereas high temperature dwells above 1000 °C can even decrease the strain to zero percent. It is important to note that isothermal holds (>10 h) below 1000 °C are required in most literature cases to guarantee full conversion of amorphous to full crystallinity which results in constant strain values for $Ce_{0.8}Gd_{0.2}O_{1.9-x}$ thin films. Time–Temperature-Transformation (TTT) diagrams give suitable engineering guidelines on the thin film characteristic transformation to full crystallinity for lattice strain engineering. *Biphasic amorphous–crystalline films* change their lattice strain values actively during crystallization. Since there is much more scope for lattice defects during crystallization while the lattices are still quite soft, higher lattice strains are reported compared to fully crystalline structures. Changes of the lattice strain of 7–1% are given in the literature for $Ce_{0.8}Gd_{0.2}O_{1.9-x}$ with respect to deposition method and annealing. Zero-strain is never achievable for biphasic thin film microstructures. Crystallization is mostly active during pure heating (3–10 K/min) of deposited thin film microstructures up to temperatures of 1000 °C and for low isothermal dwell times (<5 h).

The actual degree of remaining in amorphous phase of a thin film at deposition and its residual strain values are high for low-temperature precipitation-based deposition methods such as spray pyrolysis, flame spraying or sol–gel.

The strain levels of single-phase $Ce_{0.8}Gd_{0.2}O_{1.9-x}$ thin films differ from those of oxide films undertaking phase changes. The first Monte-Carlo simulations and experimental studies on the phase-polymorph yttria-stabilized zirconia revealed that these films change their nearest neighbor cations to compensate for strains higher than 3%. Thus, it is to be concluded through this review that $Ce_{0.8}Gd_{0.2}O_{1.9-x}$ thin films can tolerate much higher strains and distortions to study the impact on ionic diffusion than other state-of-the-art phase-polymorph ionic conductors.

When comparing with the metals literature we find that up to 2% of lattice strains are standard for metal thin films [127–130]. The lattice strain values of up to 7% here reported for the example of a single phase metal oxide are high and show the capability of ceramics to withstand high strains in the crystal lattices.

The ionic conductivity of thin films is found to vary with respect to film processing on the given example of $Ce_{0.8}Gd_{0.2}O_{1.9-x}$. It is shown that plots of *activation energy of ionic conductivity* vs. *lattice strain* correlate with the differences in ionic diffusion. A strong scatter of 1.1 ± 0.3 eV in activation energy of ionic conductivity (air) can be summarized for $Ce_{0.8}Gd_{0.2}O_{1.9-x}$ thin films in literature. Fully crystalline films show variances of up to one order of magnitude and a difference of $\Delta 0.6$ eV for lattice strain of 0.05–1%. In this instance, the variance in the ionic transport characteristics is largest for broad differences in lattice strain. Extrapolation of the activation energy to almost zero strain (0.01%) results in a processing independence and high activation energy of ionic conduction of 1.45 ± 0.05 eV. It can be concluded that for ceramic thin films, differences in the strain state exist, and that the local disorder affects the ionic transport. Strained ionic conducting thin films differ substantially from zero-strained sintered bulk ceramics.

The well-known literature hypothesis that the ionic conduction of a metal oxide is a pure scaling function of the ambient grain size on the nano-range cannot be confirmed through this literature review. Plotting literature data of differently processed $Ce_{0.8}Gd_{0.2}O_{1.9-x}$ thin films with respect to grain size it could be clearly revealed that similar grain sizes neither result in similar ionic conductivity nor in comparable activation energies. It is therefore strongly proposed to consider lattice strain as a new additional microstructural measure for characterizing the real local disorder states after film processing and annealing history in the future besides conventional ones such as grain size. Open question remains at this point how strain alters the ionic migration barrier on an atomistic level. Is it related to pure decrease in oxygen vacancy mobility of single vacancies, or do we have to take into account pairing of vacancies and hampered motion of clusters under strain? It is encouraged to assemble experimentally wise atomistic information relative to strain states for thin films. One may consider neutron diffraction experiments to probe the oxygen vacancy positions, or detailed Raman investigations to probe ionic bond length changes of the cation–anion interactions in the lattice relative to strain in future.

Electroceramic applications based on functional ionic conducting films integrated on Si-wafers benefit from careful consideration of the evolution of strain and degree of crystallinity during first heat-up and device operation. Highly strained fully crystalline thin films of increased ionic transport can be realized for Si-based electroceramic devices through reduction of the overall processing and operation temperatures over the range of 100 to 500 °C. Important is to deposit film thicknesses of the ionic conductor of more than 200 nm to avoid strong substrate impact on overall lattice strain states. It is reported through this paper that the ionic diffusion kinetics can be improved by up to one order of magnitude through distinctive thin film processing choice through *lattice strain*. In contrast to anisotropic-strained heterolayers the strained films of more than 200 nm in thickness are especially advantageous since the strain is isotropically distributed over the full volume of the film. In this case the lattice strain is no longer an interfacial substrate-film artifact. The strain is defined by the local change in ionic bond strength given through the initial thin film processing history. Thus it can be concluded that lattice strain is not interface misfit related as for heterolayers. This allows more flexible Si-based electroceramic device designs using the cross- as well as the in-plane ionic conduction characteristics of functional films in future.

Acknowledgment

Prof. Dr. Nicola A. Spaldin from the University of California Santa Barbara (USA) is thanked for stimulating discussion.

The Swiss National Science Foundation is acknowledged for the advanced researcher fellowship PA00P2-134153 for 2011/2012.

The I^2CNER and International Research Center for Hydrogen Energy, Kyushu University Japan, is thanked for the visiting associate professorship in 2011/2012.

References

[1] H.L. Tuller, R. Mlcak, Curr. Opin. Solid State Mater Sci 3 (5) (1998) 501.
[2] P. Jasinski, T. Suzuki, H.U. Anderson, Sens. Actuators, B 95 (1–3) (2003) 73.
[3] I. Kosacki, H.U. Anderson, Sens. Actuators, B 48 (1–3) (1998) 263.
[4] H. Huang, M. Nakamura, P.C. Su, R. Fasching, Y. Saito, F.B. Prinz, J. Electrochem. Soc. 154 (1) (2007) B20.
[5] D.B. Bieberle-Hütter, A. Infortuna, U.P. Muecke, J.L.M. Rupp, L.J. Gauckler, S. Rey-Mermet, P. Muralt, N.R. Bieri, N. Hotz, M.J. Stutz, D. Poulikakos, P. Heeb, P. Müller, A. Bernard, R. Gmür, T. Hocker, J. Power Sources 177 (1) (2008) 123.
[6] U.P. Muecke, D. Beckel, A. Bernard, A. Bieberle-Hütter, S. Graf, A. Infortuna, J.L.M. Rupp, J. Schneider, P. Müller, J. Gauckler, Adv. Funct. Mater. 18 (20) (2008) 3158.
[7] J.L.M. Rupp, U.P. Muecke, P.C. Nalam, L.J. Gauckler, J. Power Sources 195 (9) (2010) 2669.
[8] P.C. Su, C.C. Chao, J.H. Shim, R. Fasching, F.B. Prinz, Nano Lett. 8 (8) (2008) 2289.
[9] I. Garbayo, A. Tarancon, J. Santiso, F. Peiro, E. Alarcon-Llado, A. Cavallaro, I. Gracia, C. Cane, N. Sabate, Solid State Ionics 181 (5–7) (2010) 322.
[10] A. Evans, A. Bieberle-Hütter, H. Galinski, J.L.M. Rupp, T. Ryll, S. Barbara, R. Tölke, L.J. Gauckler, Chem. Mon. 140 (9) (2009) 975.
[11] H.L. Tuller, Solid State Ionics 131 (1–2) (2000) 143.
[12] A. Evans, A. Bieberle-Hütter, J.L.M. Rupp, L.J. Gauckler, J. Power Sources 194 (1) (2009) 119.
[13] D. Beckel, A. Bieberle-Hutter, A. Harvey, A. Infortuna, U.P. Muecke, M. Prestat, J.L. M. Rupp, L.J. Gauckler, J. Power Sources 173 (1) (2007) 325.
[14] L.Q. Chen, J. Am. Ceram. Soc. 91 (6) (2008) 1835.
[15] M. Dawber, N. Stucki, C. Lichtensteiger, S. Gariglio, J.M. Triscone, J. Phys. Condens. Matter 20 (26) (2008).
[16] O. Dieguez, D. Vanderbilt, Phase Transitions 81 (7–8) (2008) 607.
[17] J. Junquera, P. Ghosez, J. Comput. Theor. Nanosci. 5 (11) (2008) 2071.
[18] S.O. Leontsev, R.E. Eitel, Sci. Technol. Adv. Mater. 11 (4) (2010).
[19] R. Ramesh, N.A. Spaldin, Nat. Mater. 6 (1) (2007) 21.
[20] C. Ederer, N.A. Spaldin, Phys. Rev. B 71 (22) (2005).
[21] A. Kushima, B. Yildiz, J. Mater. Chem. 20 (23) (2011) 4809.
[22] A. Kushima, B. Yildiz, Y. Sindney, Phys. Rev. B 82 (2010) 115435.
[23] W. Donner, C.L. Chen, M. Liu, J. Jacobsen, Y.-L. Lee, M. Gadre, D. Morgan, Chem. Mater. 23 (4) (2011) 984.
[24] L.J. Gauckler, D. Beckel, B.E. Buergler, E. Jud, U.P. Mücke, M. Prestat, J.L.M. Rupp, J. Richter, Chimia 58 (12) (2004) 837.
[25] N.P. Brandon, S. Skinner, B.C.H. Steele, Annu. Rev. Mater. Res. 33 (2003) 183.
[26] V.V. Kharton, F.M.B. Marques, A. Atkinson, Solid State Ionics 174 (1–4) (2004) 135.
[27] M. Greenberg, E. Wachtel, I. Lubomirsky, J. Fleig, J. Maier, Adv. Funct. Mater. 16 (1) (2006) 48.
[28] I. Lubomirsky, Solid State Ionics 177 (19–25) (2006) 1639.
[29] A. Kossoy, Y. Feldman, E. Wachtel, I. Lubomirsky, J. Maier, Adv. Funct. Mater. 17 (14) (2007) 2393.
[30] I. Lubomirsky, Phys. Chem. Chem. Phys. 9 (28) (2007) 3701.
[31] A. Kossoy, Y. Feldman, R. Korobko, E. Wachtel, I. Lubomirsky, J. Maier, Adv. Funct. Mater. 19 (4) (2009) 634.
[32] I. Lubomirsky, Monatsh. Chem. 140 (9) (2009) 1025.
[33] E. Wachtel, I. Lubomirsky, Scr. Mater. 65 (2011) 112.
[34] S. Hull, S.T. Norberg, I. Ahmed, S.G. Eriksson, D. Marrocchelli, P.A. Madden, J. Solid State Chem. 182 (2009) 2815.
[35] S.T. Norberg, S. Hull, I. Ahmed, S.G. Eriksson, D. Marrocchelli, Chem. Mater. 23 (2011) 1356.
[36] D. Marrocchelli, P.A. Madden, S.T. Norberg, S. Hull, Chem. Mater. 23 (2011) 1365.
[37] P. Scherrer, Nachr. Königlichen Ges. Wiss. Göttingen Math. Phys. Kl. 1 (1918) 98.
[38] A.J.C. Wilson, Acta Crystallogr. 2 (5) (1949) 318.

[39] A. Stukowski, J. Markmann, J. Weissmuller, K. Albe, Acta Mater. 57 (5) (2009) 1648.
[40] N. Brown, K.F. Lukens, Acta Metall. 9 (1961) 106.
[41] C.H. Moelle, H.J. Fecht, Nanostruct. Mater. 6 (1–4) (1995) 421.
[42] E. Zolotoyabko, J.P. Quintana, Nucl. Instrum. Methods Phys. Res. Sect. B. Beam Interact. Mater. Atoms 200 (2003) 382.
[43] A. Stukowski, J. Markmann, J. Weissmüller, K. Albe, Acta Mater. 57 (5) (2009) 1648.
[44] S. Forest, R. Sievert, Int. J. Solids and Struct. 43 (2006) 7724.
[45] W. Hall, G.K. Williamson, Acta Metall. 1 (1953) 22.
[46] J.L.M. Rupp, B. Scherrer, L.J. Gauckler, Phys. Chem. Chem. Phys. 12 (36) (2010) 11114.
[47] W.C. Johnson, H. Schmalzried, Acta Metall. Mater. 40 (9) (1992) 2337.
[48] H. Schmalzried, React. Solids 8 (3–4) (1990) 247.
[49] H. Schmalzried, M. Backhaus-Ricoult, Prog. Solid State Chem. 22 (1) (1993) 1.
[50] R. Röttger, H. Schmalzried, Solid State Ionics 150 (1–2) (2002) 131.
[51] Y.M. Chiang, E.B. Lavik, I. Kosacki, H.L. Tuller, J.Y. Ying, Appl. Phys. Lett. 69 (2) (1996) 185.
[52] J.-M. Chiang, E.B. Lavik, I. Kosacki, H.L. Tuller, J. Electroceram. 1 (1) (1997) 7.
[53] P. Knauth, H.L. Tuller, Solid State Ionics 136 (2000) 1215.
[54] I. Kosacki, T. Suzuki, V. Petrovsky, H.U. Anderson, Solid State Ionics 136 (2000) 1225.
[55] I. Kosacki, T. Suzuki, H.U. Anderson, P. Colomban, Solid State Ionics 149 (1–2) (2002) 99.
[56] X.-D. Zhou, W. Huebner, I. Kosacki, H.U. Anderson, J. Am. Ceram. Soc. 85 (7) (2002) 1757.
[57] J.L.M. Rupp, A. Infortuna, L.J. Gauckler, J. Am. Ceram. Soc. 90 (6) (2007) 1792.
[58] J.L.M. Rupp, L.J. Gauckler, Solid State Ionics 177 (2006) 2513.
[59] M. Mogensen, N.M. Sammes, G.A. Tompsett, Solid State Ionics 129 (1–4) (2000) 63.
[60] T. Ryll, J.L.M. Rupp, A. Bieberle-Hutter and L.J. Gauckler, Crystallization, microstructure and electrochemical properties of lanthanum nickelate thin films deposited by spray pyrolysis. Acta Materialia, in review
[61] T. Ryll, A. Brunner, S. Ellenbroeck, A. Bieberle-Huetter, J.L.M. Rupp, L.J. Gauckler, Crystallization and electrical conductivity of amorphous bismuth ruthenate thin films deposited by spray pyrolysis, Phys. Chem. Chem. Phys. 12 (42) (2010) 13933.
[62] A.F. Bower, Applied Mechanics of Solids: Chapter 3 — Constitutive Models Relations between Stress and Strain, CRC Press, 2009 97814339802472.
[63] J.A. Kilner, Nat. Mater. 7 (11) (2008) 838.
[64] J. Garcia-Barriocanal, A. Rivera-Calzada, M. Varela, Z. Sefrioui, E. Iborra, C. Leon, S.J. Pennycook, J. Santamaria, Science 321 (5889) (2008) 676.
[65] N. Schichtel, C. Korte, D. Hesse, J. Janek, Phys. Chem. Chem. Phys. 11 (17) (2009) 3043.
[66] S. Sanna, V. Esposito, A. Tebano, S. Licoccia, E. Traversa, G. Balestrino, Small 6 (17) (2010) 1863.
[67] Y.G. Wang, L.A. An, L.V. Saraf, C.M. Wang, V. Shutthanandan, D.E. McCready, S. Thevuthasan, J. Mater. Sci. 44 (8) (2009) 2021.
[68] D. Pergolesi, V. Esposito, A. Tebano, P.G. Medaglia, S. Sanna, S. Licoccia, G. Balestrino, E. Traversa, in: K. Eguchi (Ed.), Solid Oxide Fuel Cells, 10, 2007, p. 891.
[69] S. Sanna, V. Esposito, D. Pergolesi, A. Orsini, A. Tebano, S. Licoccia, G. Balestrino, E. Traversa, Adv. Funct. Mater. 19 (11) (2009) 1713.
[70] A. Cavallaro, M. Burriel, J. Roqueta, A. Apostolidis, A. Bernardi, A. Tarancon, R. Srinivasan, S.N. Cook, H.L. Fraser, J.A. Kilner, D.W. McComb, J. Santiso, Solid State Ionics 181 (13–14) (2010) 592.
[71] M. Sillassen, P. Eklund, N. Pryds, E. Johnson, U. Helmersson, J. Bottiger, Adv. Funct. Mater. 20 (19) (2010) 3194.
[72] A. Kossoy, A.I. Frenkel, Q. Wang, E. Wachtel, I. Lubomirsky, Adv. Mater. 22 (14) (2010) 1659.
[73] S. Swaroop, M. Kilo, A.E. Kossoy, I. Lubomirsky, I. Riess, Solid State Ionics 179 (21–26) (2008) 1205.
[74] A. Tarancon, N. Sabate, A. Cavallaro, I. Gracia, J. Roqueta, I. Garbayo, J.P. Esquivel, G. Garcia, C. Cane, J. Santiso, J. Nanosci. Nanotechnol. 10 (2) (2010) 1327.
[75] D.J. Quinn, B. Wardle, S.M. Spearing, J. Mater. Res. 23 (3) (2008) 609.
[76] J. Santiso, M. Burriel, J. Solid State Electrochem. 15 (2011) 985.
[77] H.R. Kim, J.C. Kim, K.R. Lee, H.I. Ji, H.W. Lee, J.H. Lee, J.W. Son, Phys. Chem. Chem. Phys. 13 (2011) 6133.
[78] B. Scherrer, A. Rossi, J. Martynczuk, M.D. Rossell, A. Bieberle-Hütter, J.L.M. Rupp, R. Erni, L.J. Gauckler, J. Power Sources 196 (18) (2011) 7372.
[79] J. Will, A. Mitterdorfer, C. Kleinlogel, D. Perednis, L.J. Gauckler, Solid State Ionics 131 (1–2) (2000) 79.
[80] A. Kushima, B. Yildiz, J. Mater. Chem. 20 (23) (2010) 4809.
[81] S. Heiroth, R. Frison, J.L.M. Rupp, T. Lippert, E. Barthazy, E. Müller, K. Conder, A. Wokaun, L.J. Gauckler, Solid State Ionics 191 (1) (2011) 12.
[82] S. Heiroth, T. Lippert, A. Wokaun, M. Döbeli, J.L.M. Rupp, B. Scherrer, L.J. Gauckler, J. Eur. Ceram. Soc. 30 (2) (2010) 489.
[83] B. Scherrer, J.L.M. Rupp, A. Bieberle-Hutter, L.J. Gauckler, Adv. Funct. Mater. 21 (2011) 3967.
[84] A. Tschope, R. Birringer, J. Electroceram. 7 (3) (2001) 169.
[85] A. Tschope, E. Sommer, R. Birringer, Solid State Ionics 139 (3–4) (2001) 255.
[86] M.C. Gobel, G. Gregori, X.X. Guo, J. Maier, Phys. Chem. Chem. Phys. 12 (42) (2010) 14351.
[87] J. Maier, Solid State Ionics 157 (1–4) (2003) 327.
[88] J. Maier, Ionic Transport in Nano-sized Systems, Elsevier Preprint, 2003.
[89] J. Maier, Z. Phys. Chem. 217 (2003) 415.
[90] J. Maier, J. Eur. Ceram. Soc. 24 (6) (2004) 1251.
[91] P.S. Patil, Mater. Chem. Phys. 59 (3) (1999) 185.
[92] N. Jordan, W. Assenmacher, S. Uhlenbruck, V.A.C. Haanappel, H.P. Buchkremer, D. Stover, W. Mader, Solid State Ionics 179 (21–26) (2008) 919.
[93] K. Rodrigo, S. Heiroth, M. Dobeli, N. Pryds, S. Linderoth, J. Schou, T. Lippert, J. Optoelectron Adv. Mater. 12 (3) (2010) 511.
[94] C. Brahim, A. Ringuede, E. Gourba, M. Cassir, A. Billard, P. Briois, J. Power Sources 156 (1) (2006) 45.
[95] E. Gourba, P. Briois, A. Ringuede, M. Cassir, A. Billard, J. Solid State Electrochem. 8 (9) (2004) 633.
[96] X.N. Jiang, H. Wang, X.Y. Ma, X.Q. Meng, Q.Y. Zhang, Acta Phys. Sin. 57 (3) (2008) 1851.
[97] Y.L. Kuo, C. Lee, Y.S. Chen, H. Liang, Solid State Ionics 180 (26–27) (2009) 1421.
[98] H.Z. Song, H.B. Wang, S.W. Zha, D.K. Peng, G.Y. Meng, Solid State Ionics 156 (3–4) (2003) 249.
[99] H.B. Wang, H.Z. Song, C.R. Xia, D.K. Peng, G.Y. Meng, Mater. Res. Bull. 35 (14–15) (2000) 2363.
[100] E. Ballee, A. Ringuede, M. Cassir, M. Putkonen, L. Niinisto, Chem. Mater. 21 (19) (2009) 4614.
[101] E. Gourba, A. Ringuede, M. Cassir, J. Paivasaari, J. Niinisto, M. Putkonen, L. Niinisto, in: S.C. Singhal, M. Dokiya (Eds.), Solid Oxide Fuel Cells, VIII, 2003, pp. 267–274.
[102] D. Perednis, L.J. Gauckler, Solid State Ionics 166 (3–4) (2004) 229.
[103] P. Bohac, L. Gauckler, Solid State Ionics 119 (1–4) (1999) 317.
[104] J. Markmann, A. Tschope, R. Birringer, Acta Mater. 50 (6) (2002) 1433.
[105] S.-G. Kim, S.P. Yoon, S.W. Nam, S.-H. Hyun, S.-A. Hong, J. Power Sources 110 (1) (2002) 222.
[106] N.I. Karageorgakis, A. Heel, J.L.M. Rupp, M. Aguirre, T. Graule, L.J. Gauckler, Adv. Funct. Mater. 21 (3) (2010) 532.
[107] G. Chiodelli, L. Malavasi, V. Massarotti, P. Mustarelli, E. Quartarone, Solid State Ionics 176 (17–18) (2005) 1505.
[108] A. Infortuna, A.S. Harvey, L.J. Gauckler, Adv. Funct. Mater. 18 (1) (2008) 127.
[109] J.H. Joo, G.M. Choi, J. Eur. Ceram. Soc. 27 (13–15) (2007) 4273.
[110] J.H. Shim, C.-C. Chao, H. Huang, F.B. Prinz, Chem. Mater. 19 (2007) 3850.
[111] S. Rey-Mermet, P. Muralt, Solid State Ionics 179 (27–32) (2008) 1497.
[112] J.H. Joo, G.M. Choi, J. Power Sources 182 (2) (2008) 589.
[113] H.S. Noh, J.W. Son, H. Lee, H.S. Song, H.W. Lee, J.H. Lee, J. Electrochem. Soc. 156 (12) (2009) B1484.
[114] Y. Jee, S. Lah, J.W. Son, S.W. Cha, Curr. Appl. Phys. 10 (2010) S29.
[115] T. Suzuki, I. Kosacki, H.U. Anderson, Solid State Ionics 151 (1–4) (2002) 111.
[116] J.L.M. Rupp, A. Infortuna, L.J. Gauckler, Acta Mater. 54 (7) (2006) 1721.
[117] A. Tschope, Solid State Ionics 139 (3–4) (2001) 267.
[118] J.-H. Hwang, D.S. McLachlan, T.O. Mason, J. Electrochem. Soc. 3 (1) (1999) 7.
[119] G.M. Christie, F.P.F. van Berkel, Solid State Ionics 83 (1–2) (1996) 17.
[120] T. Suzuki, I. Kosacki, H.U. Anderson, P. Colomban, J. Am. Ceram. Soc. 84 (9) (2001) 2007.
[121] J.L.M. Rupp, B. Scherrer, N. Schäuble, L.J. Gauckler, Adv. Funct. Mater. 20 (17) (2010) 2807.
[122] H. Yahiro, K. Eguchi, H. Arai, Solid State Ionics 36 (1–2) (1989) 71.
[123] T. Inoue, T. Setoguchi, K. Eguchi, H. Arai, Solid State Ionics 35 (3–4) (1989) 285.
[124] L. Chen, C.L. Chen, X. Chen, W. Donner, S.W. Liu, Y. Lin, D.X. Huang, A.J. Jacobson, Appl. Phys. Lett. 83 (23) (2003) 4737.
[125] J.L.M. Rupp, B. Scherrer, A. Harvey, L.J. Gauckler, Adv. Funct. Mater. 19 (17) (2009) 2790.
[126] P. Lukás, Z. Kouril, P. Strunz, P. Mikula, M. Vrána, V. Wagner, Physica B 234–236 (1997) 956.
[127] H. Gleiter, J. Weissmuller, O. Wollersheim, R. Wurschum, Acta Mater. 49 (4) (2001) 737.
[128] Weissmüller, Physica B (1995) 105.
[129] H. Natter, M.-S. Loffler, C.E. Krill, R. Hempelmann, Scr. Mater. 44 (8–9) (2001) 2321.
[130] C. Korte, A. Peters, J. Janek, D. Hesse, N. Zakharov, Phys. Chem. Chem. Phys. 10 (2008) 4623.
[131] C. Kleinlogel, L.J. Gauckler, Solid State Ionics 135 (1–4) (2000) 567.
[132] E. Jud, L.J. Gauckler, J. Electroceram. 15 (2) (2005) 159.
[133] D. Schneider, M. Godickemeier, L.J. Gauckler, J. Electroceram. 1 (2) (1997) 165.
[134] J.L.M. Rupp, C. Solenthaler, P. Gasser, U.P. Muecke, L.J. Gauckler, Acta Mater. 55 (10) (2007) 3505.